LAue Cu Lens imaging and POLarimetry with CAdmium telluride Array (LA-POLCA)

Experiment No MI-905 Report

***Proposer*:**
Ezio CAROLI, INAF/IASF-Bologna, Via Gobetti 101, Bologna, Italy

Co-proposers:
Carlos Alberto Nabais CONDE, Dep. de Fisica, Universidade de Coimbra, Portugal
Rui Miguel CURADO DA SILVA, Dep. de Fisica, Universidade de Coimbra, Portugal
Stefano DEL SORDO, INAF/IASF-Palermo, Italy
Filippo FRONTERA, Dip. di Fisica, Università di Ferrara, Italy
Veijo HONKIMAKI, ESRF, Grenoble, France
Alessandro PISA, Dip. di Fisica, Università di Ferrara, Italy
John Buchan STEPHEN, INAF/IASF-Bologna, Italy
Giulio VENTURA, INAF/IASF-Bologna, Italy

Participants to beam tests:
Ezio Caroli, INAF/IASF-Bologna, Italy
John Buchan Stephen, INAF/IASF-Bologna, Italy
Stefano del Sordo, INAF/IASF-Palermo, Italy
Natalia Auricchio, Dip. di Fisica, Università di Ferrara, Italy
Alessandro Pisa, Dip. di Fisica, Università di Ferrara, Italy
Rui Miguel Curado da Silva, Dep. de Fisica, Universidade de Coimbra, Portugal

Beamline:	ID 15B
Responsible:	Dr. Veijo Honkimaki
Shift Period:	29 February -04 March 2008
Number of shift:	6

Table of contents

1 INTRODUCTION

The experiment is a collaboration project between the INAF/IASF – Bologna and Palermo and the University of Ferrara, Italy, and the Dep. de Física da Universidade de Coimbra. The aim of this project is to optimize the design of CZT/CdTe pixel detectors for hard X and soft γ-ray astrophysics for performing high sensitivity polarimetric measurements together with spectroscopy, imaging and timing in the 100 keV – 1 MeV range. This idea was born several years ago [1,2] with a view to implementation in a new generation of wide field telescope, but it has, more recently, become very appealing within the framework of the new ESA plan for the next decade (Cosmic Vision 2015-2025). In fact polarimetry has been recognized as a very important observational parameter also for high energy astrophysics (>100 keV) and therefore this capability should be included in proposals for future space missions [3]. In particular the proposers have been involved, as part of a large European collaboration, in the preparation of a new telescope mission concept (GRI, Gamma Ray Imager) based on Laue focussing techniques [4]. The GRI mission proposal has been submitted in June 2007 in answer to ESA Cosmic Vision 2015-2025 first call for proposal. Even if the proposal have not been selected in this run, it has been recognized as an extremely challenging idea and technology for future high sensitivity hard X and soft gamma-ray mission. In this perspective and for ongoing development activities on Laue lens for hard X- and soft gamma-rays astrophysics [5,6,7], the data obtained by the LA-POLCA experiment (MI-905) at ESRF are very important for optimizing the design of a Laue lens high efficiency focal plane based on CZT pixel detector in order to obtain the best performance also as a Compton scattering hard X- and soft γ-ray polarimeter.

In particular the LaPOLCA experiment has been conceived to test the coupling between room temperature operating CZT pixel detector with a wide energy band Laue lens made of copper mosaic crystals and to evaluate possible systematic effects on the incoming beam polarisation status introduced by the diffraction process through the mosaic crystal structure.

This experiment is a logic follow-up of the research activity started several years ago with the development of a sophisticated Monte Carlo simulation code based on the GEANT4 environment, already used to perform an extensive study of the expected response and performance of CZT/CdTe pixel spectrometers used as scattering polarimeters [8]. In order to compare and calibrate the simulations with measurements, a first experiment (POLCA/MI-592) was already implemented at the ERSF-ID 15 beamline in July 2002 [9,10]. Encouraged by these results, the a new larger size experiment (POLCA II/MI-857, February 2007) has given us more information about the dependence of the polarisation modulation factor on the incoming photon energy in the range 100-1000 keV [11, 12].

2 EXPERIMENT DESCRIPTION AND SET UP AT THE BEAM LINE ID15B

The LaPOLCA experiment was set-up in the experimental hutch at about ~5 m from the beam entrance window on a micrometric positioning and rotation system (see below).
The experiment we performed was based on three main subsystems: **1** the beam line, **2** the Laue Lens simulator (Cu crystals, named as LL in the following) and **3** the POLCA detection system. The general LA-POLCA experiment set-up scheme is shown in Figure 1.

All the LA-POLCA subsystems (detector, power supply, multiparametric electronics, Laue lens simulator) have been mounted inside the experimental hutch, leaving in the control room only the NI PXI box with the NI 6533 data acquisition board, the ESRF control console and the Quick-look station (PC) (Figure 2).

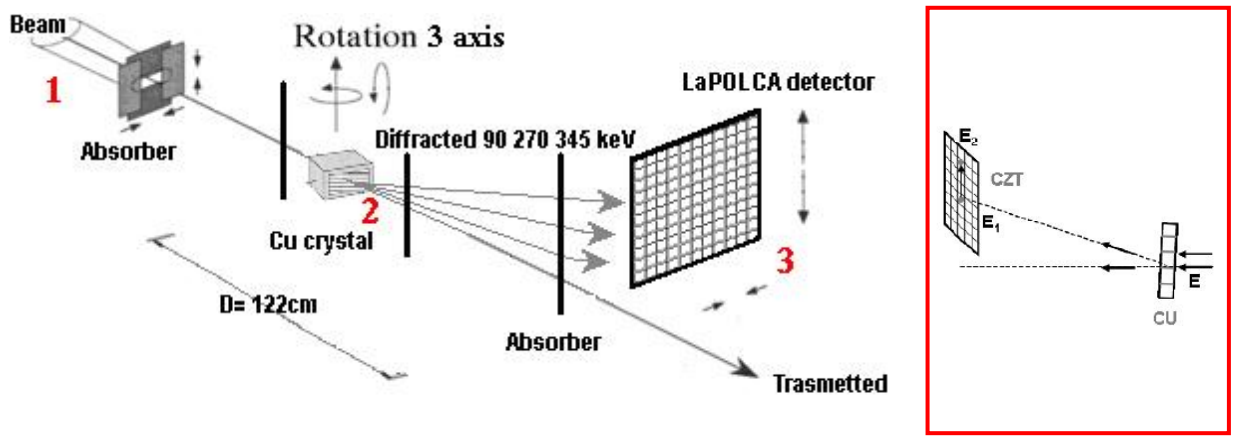

Figure 1. *LaPOLCA experiment set-up scheme. On the right (red box), the CZT detector surface where is represented a double event: i.e. an event that is scattered from the beam target pixel to a separate one losing respectively energy E1 and E2 in the two hits.*

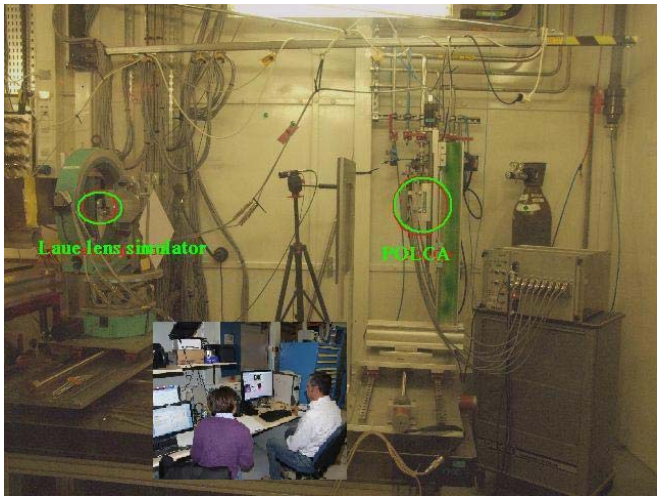

Figure 2. *LA-POLCA Experiment at ESRF: the ID 15B experimental hutch where the two main subsystems are shown (large image) and the quick-look station in the control room (window image).*

2.1 The ID 15B beam

The ID15B beam line at ESRF allows the production of polychromatic (100%) linearly polarised radiation at energies of ~90 keV, 270 keV, 345 keV, and superior harmonics (with very low intensity and outside the detector response dynamics) with a square spot diameter of 0.3×0.3 mm^2.

0.3×0.3 mm spot size
~100% linear polarized
Polychromatic beam: 90 keV primary, 270 keV (3^{rd} harmonics), 345 keV (4^{th} harmonics).
Beam attenuator: Pb (5 mm, 4 mm @ 345 keV) + Cu (3 mm)

Table I. *Beam Characteristics.*

In order to avoid signal-pileup and dead time increase in the detection electronics because of the high beam intensity we have used during all the measurements a graded shield made of Pb/Cu at the beam entrance in the experiment hutch. With this shield we were able to limit the detector count rate always below 15000 c/s. The details of the passive shield used are reported in Table V. The relatively low intensity of the diffracted beam @ 90 keV with respect to 270 keV is due to the presence of attenuator (Pb+Cu) between the beam and the Cu crystal 90 keV.

Figure 3 shows the transmitted beam as seen by pixel 201 of the CZT detector at the first two allowed harmonics (1st and 3rd, the 2nd being forbidden by the Ge mono-chromator used to produce the beam at ID15B). The fourth beam harmonic at 345 keV was also used after substituting the 12 kΩ resistors with 15 kΩ on the detector data cables in order to increase the operational energy dynamics.

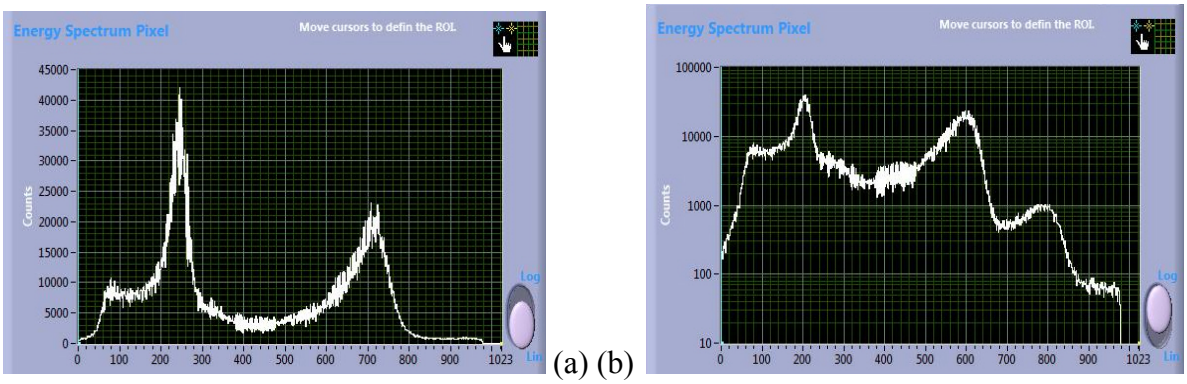

Figure 3. *Transmitted (through the Cu mosaic crystal) beam spectra (accumulated in 1000 s) impinging over pixel 201 with two different gain to change the detector dynamics. (a) high gain measurement: only the 1st and the 3rd armonics (90 and 270 keV) are detected; (b) low gain measure with all the first three allowed armonics (90, 270, and 345 keV) of the diffracted beam are visible.*

During the Laue lens simulation measurements, we have used a thick shield made by Pb (10 cm thick) bricks positioned close to the Cu crystal in order to completely absorb the transmitted beam and to be sure that do not intercept the POLCA detector in any position.

2.2 LaPOLCA detection systems

The detection system is schematically represented in Figure 4 and comprises the pixel spectrometer with the analogue front end electronics, the data processing electronics and the data acquisition system.

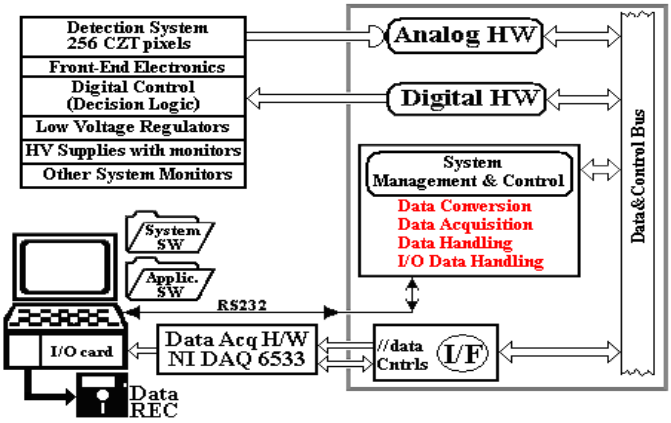

Figure 4. *The functional scheme of the detection system: (left top box) the CZT pixel detector with the Analogue front-end electronics; (right box) the multiparametric data processing electronics; (bottom right icons) the data acquisition system.*

The detector used for the LaPOLCA experiment is an improved version (Figure 5) of the POLCA II detector and is based on a 5 mm thick CZT crystal with the anode segmented into 16×16 pixels (2.5×2.5 mm^2) from Imarad (Israel) [13]. In the current configuration only an array of 11×11 pixels (sensitive area of 3×3 cm^2) is connected to the readout electronics. The pixel readout is provided by eight eV PRODUCTS 16-channel ASICs with peaking time set at 1.2 μs. The HV bias for the detector (-600 V) is provided by a DC-DC converter (EMCO), while the low tensions for both the ASIC's board and the DC-DC converter are generated by an external custom made power unit. The multiparametric back-end electronics is able to read up to 128 independent channels with filters, coincidence logic and ADC units. This system is connected, through a high speed 32 bit parallel NI-DIO/PXI board, to a PC with quick-look and storage s/w developed in LABVIEW.

(a) 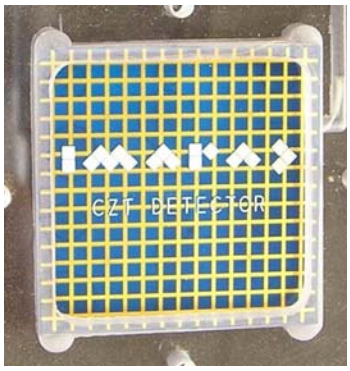

(b) 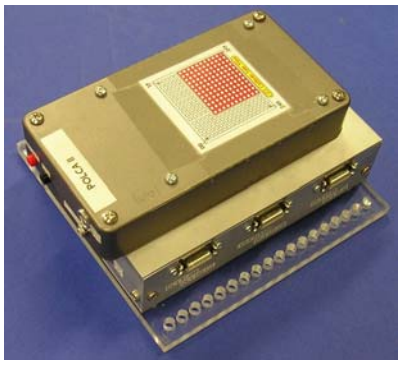
(c)


2.3 The Laue lens simulator

An LL is a set of properly oriented crystals. In our experiment it was emulated by using a single crystal that was rotated and placed in the correct positions in front of the beam. The Cu crystal was mounted on a 3 axis linear motion stage coupled with a 2 axis rotation stage to properly align the Cu crystal 111 surface (Figure 6) with respect to the incident beam and to

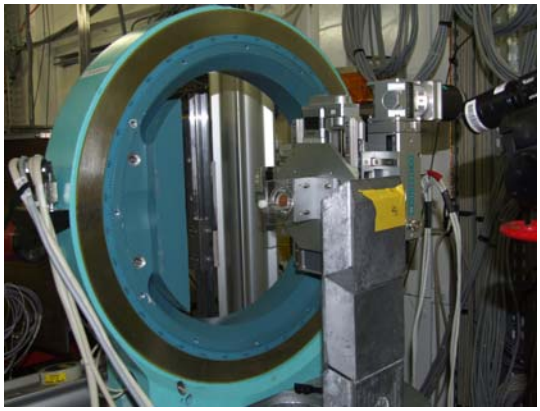
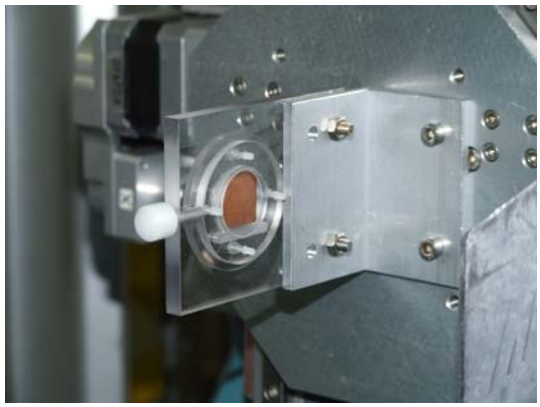

Figure 6. *The large blue ring (left) provide the rotation around directions parallel to the beam axis, while the small rotation stage below the crystal support allow to modify the angle between the beam and the Cu crystal surface. The XYZ translator allows re-centring the crystal with respect to the beam after each movement and rotation. The Lead brick shield used to stop the transmitted beam is visible. The Laue lens simulator basic element (right), i.e. the mosaic Cu crystal provided by ILL in Grenoble, inside the Plexiglas support.*

perform the rotation of the crystal itself around the virtual axis of the LL. In this way it was possible to emulate the equivalent of three Laue rings - one for each available energy.

Furthermore, the advantage of emulating a LL with one crystal is that the mosaic structure is fixed, therefore avoiding additional effects due the intrinsic spread of this structure in a Cu crystal sample. The Cu crystal (4 mm thick and 15×15 mm^2 in surface) was provided by the Institute Laue-Langevin (ILL) in Grenoble in a sample of about 25 units used at the University of Ferrara to build a Laue lens demonstration model. Figure 6 (right) shows the Cu crystal inside the Plexiglas support built to connect it to the micro positioning system. The Cu crystal is

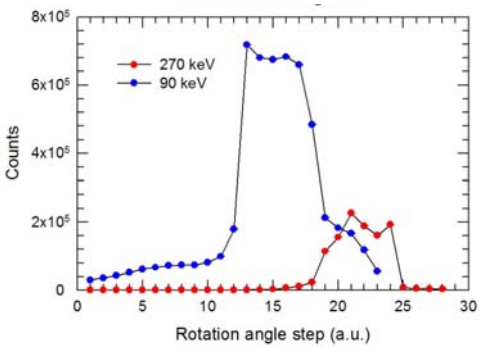

Figure 7. *The Cu crystal rocking curve obtained at two beam energies.*

characterised by the rocking curve (integrated diffracted beam intensity vs. crystal surface orientation) shown in Figure 7 and obtained at the ID15B beam line using the 90 keV and 270 keV lines with rotation steps of 36". These curves were used to evaluate the mosaicity level of the crystal, and the value of ~3' (Full Width Half Maximum) is in close agreement with the value reported by the ILL.

3 THE LAPOLCA TESTS

The experiment had two main strictly related targets:

(a) to demonstrate that the combination of a Laue Lens (LL), built with copper crystals with a CZT/CdTe pixel detector, is able to perform high sensitivity measurement of the polarization of an hard X ray sources contemporary with spectroscopy and imaging of the same source;
(b) to evaluate possible systematic effects on the polarisation status of incoming photons introduced by the Laue diffraction process.

This chapter will describe the LaPOLCA performed tests using the beam line ID 15B at the ESRF. For each test type the objective as well as the required set up and measurement condition and typical integration time are given.
The measurements was divided in two main classes: (a) Simulation of Laue lens rings; (b) Polarimetry with a polychromatic beam.

3.1 Pixel scans for response non uniformity correction.

These are preliminary measurements performed in order to determine the response of each LaPOLCA pixel at selected energies and to allow during the polarisation data analysis to normalize the pixels response. In particular the single events acquired during these tests will be used to correct the double event data for efficiency and gain non uniformity across the active detector surface.

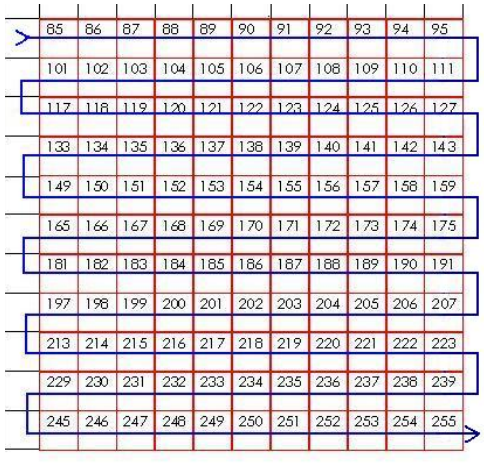

Figure7*. The path used during the pixel scan tests performed to make relative efficiency correction during the data analysis.*

This test type consist of scans over all the 11×11 detector pixels with a fine (0.5 mm diameter) collimated beam for each energy that will be used for polarimetric measurements.
At a given energy each scan start at the centre of pixel at the left of the left top corner pixel of the active detector array, and then using the *XY* micrometric positioning system the detector was moved in order to scan all the pixels following a path like the one shown in Figure 7. The measurement time at each reached pixel was, generally, set to 20 s in order to have enough statistics: assuming an average count rate of 1000 c/s (consistent with 90 and 270 keV diffracted beam intensities), we will acquire ~2×10^4 counts, this number of course depending on the beam energy.
We point out that the introduction of a time counter in the TAKES output data words have allowed the implementation of scan macro that can cover the entire active detector surface. In fact using this time information it is possible to reconstruct more precisely the number of events accumulated when the beam is just centred on each pixel, discarding all counts accumulated when the beam is actually moving from a pixel through to the subsequent one.

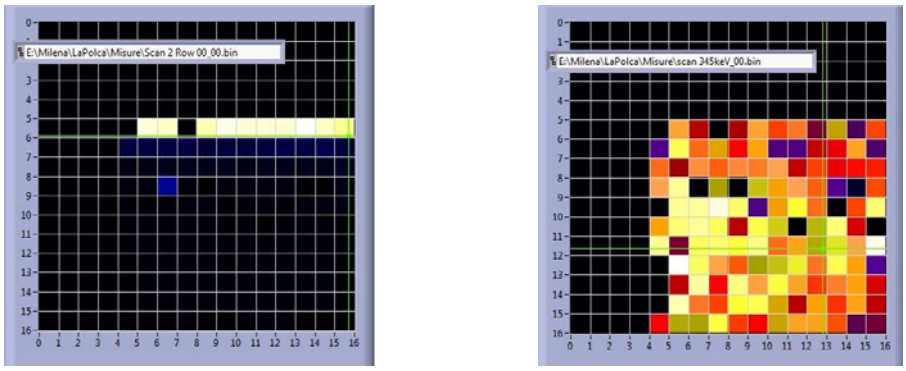

Figure 8. *(left) Single row scan and (right) the results of a complete detector scan.*

This type of measurements have been repeated at the begin of each Laue lens ring simulation and each polarisation measurement. The detector count maps during a typical scan test are showed in Figure 8.

3.2 Simulation of a Laue lens ring

For each available energy in the incoming beam, we found the Laue diffraction condition for the given Cu crystal 111 surfaces. We then rotated the crystal around directions parallel to the axis beam to simulate a Laue ring (Figure 9) comprising 16 elements (one every 22º.5).

For each Cu crystal configuration the detector was moved in order to intercept the diffracted beam always with the same pixel (201) in the central part of the sensitive surface. In this way it was possible to emulate the equivalent of three Laue rings one for each available energy lines. Furthermore, the advantage of emulating a LL with one crystal is that the mosaic structure is fixed, therefore avoiding additional effects due the intrinsic spread of this structure in a Cu crystal sample.

Figure 10 shows the diffracted beam as seen by pixel 201 of the CZT detector at 270 keV. In Figure 11 the detected monochromatic diffracted spectra at the first three allowed harmonics (1^{st} and 3^{rd}, and 4^{th}, the 2^{nd} being forbidden by the Ge mono-chromator used to produce the beam at ID15B). The fourth beam harmonic at 345 keV was obtained after substituting the 12 kΩ resistors with 15 kΩ on the detector data cables in order to increase the operational energy dynamics.

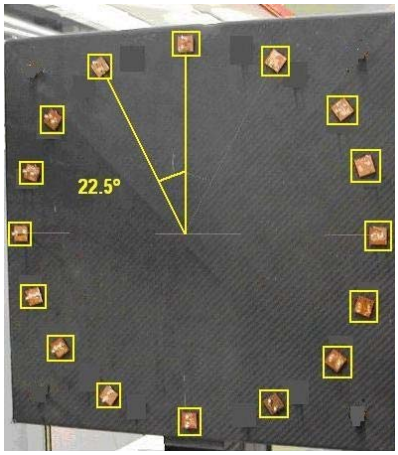

Figure 9. *A reconstruction of the simulated 16 elements Laue lens ring during the test using as background the carbon fiber support of the demonstration model built at the Ferrara University.*

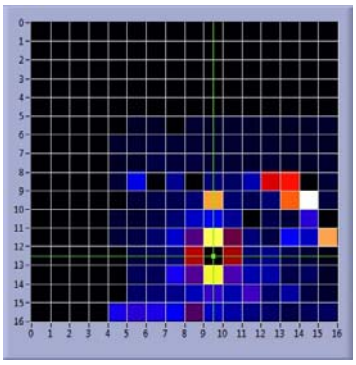

Fig. 10. *The diffracted beam impinging on pixel 201 centre.*

The detected intensities of the three diffracted beam lines were indicatively: ~950 c/s at 90 keV, ~1500 c/s at 270 and only 85 c/s at 345 keV. The relatively low intensity of the diffracted beam at 90 keV can be mainly attributed to the higher stopping efficiency of the Pb (5 mm thick)/Cu (4 mm thick) shield at the beam entrance in the experiment hutch (used to limit the incoming flux in order to avoid signal-pileup and dead time increase in the detection electronics) and higher self absorption across the 4 mm thickness of the Cu crystal at this energy with respect to the higher one: at 90 keV about 85% of the incoming beam is absorbed while at 270 keV this percentage is only 47%.

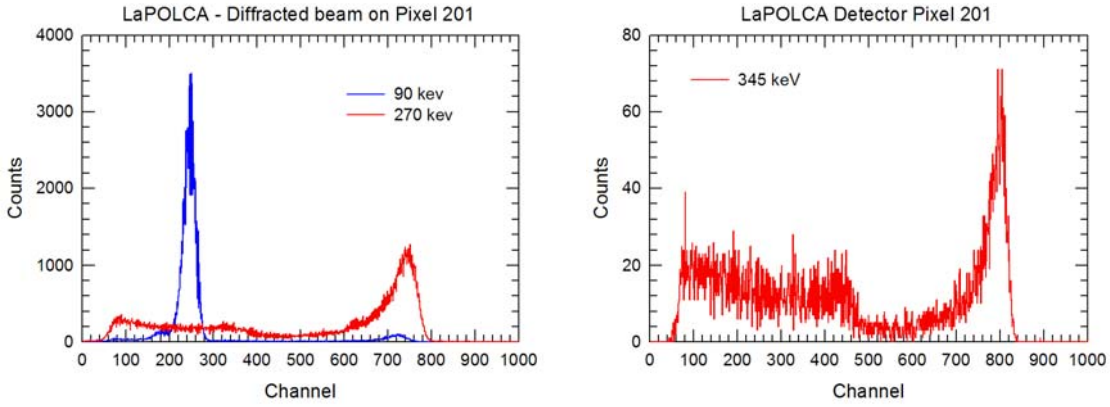

Figure 11. *The spectra of the diffracted beam as detected by the pixel 201 of the CZT detector for 90 keV and 270 and 345 keV incident beam harmonics. The acquisition time is 120 s.*

3.3 Polarimetry tests

These tests set have the aim to make a confirmation of the polarimetric performance of our pixel CZT detector obtained with the POLCA II experiment in February 2007.
The tests will be made using the fine collimated diffracted beam the three available energies centred at on each of the four corner pixel, 85, 95, 245, 255, of the active detector (Figure 7).
The calculation of the modulation Q factor depends on the double events distribution and statistics. In order to get enough statistics on double events these test will require a relative large integration time for each measure. Because typically we expect double event percentage between few percent at the lower beam energy and up to ~10% at the higher one, we need to collect ~10^6 counts to have a least 10^5 double events, e.g. less than 0.5 % as statistic error. Taking as average rate 1000 c/s for all the available energies, an integration time of 1000 s for each irradiating configuration was used (Figure 12).

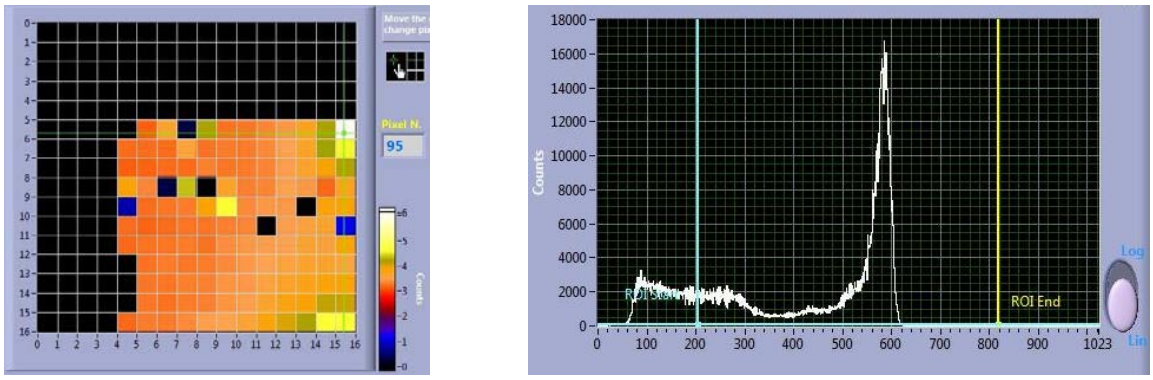

Figure 12. *(left) Counts distribution map (in logarithmic false color scale) with the diffracted beam impinging on pixel 95; (right) the pixel 95 energy spectrum for the beam energy of 270 keV (3rd armonics).*

4 RESULTS SUMMARY

The results of the LaPOLCA experiment was preliminary presented in October 2008 at the IEEE Nuclear Science Symposium [14] and published in the IEEE TNS journal [15].

4.1 Pixel efficiency normalisation

In order to perform a reliable evaluation of the performance of a detector used as a scattering polarimeter it is very important to remove sources of systematic errors. In a CZT pixel detector one of the most important effects that can severely degrade the polarimetric response is the non uniformity in the pixel response. The distributions of the relative detection

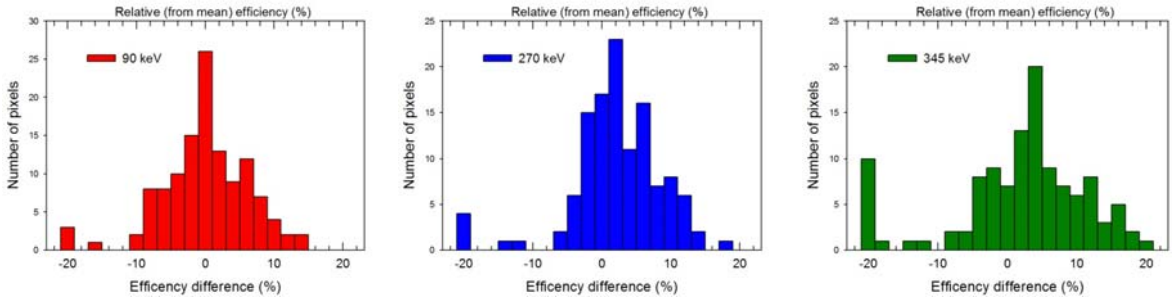

Figure 13. *The distribution of the difference from the average value of the single event relative detection efficiency for all the pixels measured at the three beam energy.*

efficiency across all the pixels for single events (i.e. events that trigger only one pixel inside the set coincidence window) for the diffracted beam at the three energies (90, 270 and 345 keV is shown in Figure 13. Typically the detection non uniformity (using counts integrated over the entire detected spectrum) is within ±10% for most (~90%) of the pixels, reaching ±20% for the remainder. The characteristics of this distribution are almost equivalent for all the tested energies.

A simple method to correct for this non uniformity is provided by the use of the following ratio calculated from the single events count in each pixel:

$$f_i = \frac{N_{sMax}}{(N_{sng})_i} \tag{1}$$

where N_{sMax} is the maximum single event count and $(N_{sng})_i$ is the single event counts in the i-th pixel. In particular this ratio will be applied to normalize the double events count rate attributed to each pixel before the evaluation of the polarimetric performance (see following section).

4.2 Double event efficiency

The performance of a scattering polarimeter relies on the distribution of the scattering directions of events that undergo a Compton interaction in one pixel and full absorption in a second, separate, pixel. The polarimetric sensitivity of such a detector is strongly dependent on the efficiency in the detection of Compton scattered events, that we refer to as double events.

Of course the high Z of CZT strongly limits the detection efficiency of double events, because the Compton cross section starts to become effective with respect to photoelectric absorption above 80 keV. Furthermore, because the mean free path of photons is very short at low energies (<100 keV), the finite pixel dimension (2.5 mm in our case) produces a further decrease in the observed double-event counts due to absorption of the scattered photon in the same pixel. This is clearly evident in the data of Figure 14, where the relative double-event efficiencies (integrated over the entire detected diffracted spectrum at each beam energy and for a 4μs coincidence window) for each Cu crystal position are reported. The double event efficiency at 90 keV is just around 0.15%, almost two orders of magnitude lower with respect to the values measured at the higher energies.

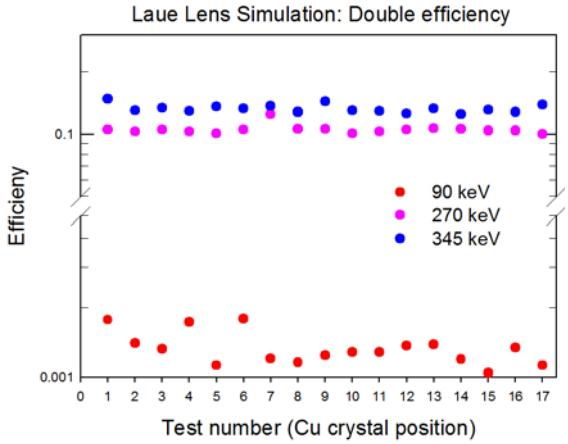

Figure 14. *The double event efficiency as measured for each Cu crystal position during the Laue lens simulation tests. The plotted data have been normalized using the correction factors evaluated by using (1).*

4.3 Polarimetric modulation factor evaluation

The polarisation status of photons will produce on the Compton scattered events distribution a typical asymmetry. After undergoing Compton scattering, the polarized photons' new direction depends on the orientation of its polarization vector before the interaction. If the polarized scattered photons go through a new interaction inside the detector, the statistical distribution of the relative positions of the two interactions (double event) allows us to infer the degree and polarization direction of the incident radiation. The Klein–Nishina cross section σ per solid angle (Ω) unit for linearly polarized photons is defined by:

$$\frac{d\sigma}{d\Omega} = r_0^2 \left(\frac{E'}{E}\right)^2 \left[\frac{E}{E'} + \frac{E'}{E} - 2\sin^2\vartheta\cos^2\varphi\right] \qquad (2)$$

where r_0 is the classical electron radius, E and E' are the energies of the incoming and outgoing photons, θ is the angle of the scattered photon, and φ is the angle between the scattering plane defined by the incoming and outgoing photon directions and the incident polarization plane defined by the polarization vector and the direction of the incoming photon. The maximum relative difference between the cross-section values arises for φ=0° (minimum) and φ=90° (maximum). Furthermore the relative difference is maximized for an angle θ_M dependent on the incident photon energy. For soft γ- and hard X-rays (0.1–1 MeV) the θ_M value is about 90°. The consequence of Eq. (2) for polarized photons impinging on a pixel detector is a distribution of the Compton scattered events that has an elliptical shape with respect to the circular one expected for non polarized photons. The ellipse major axis direction is orthogonal to the photon polarisation field vector: i.e. more counts are expected in this direction with respect to the minor axis direction.

The capability to measure this asymmetry defines a detector as a scattering polarimeter. The parameter that gives the quality of a detector used as a scattering polarimeter is the modulation factor Q that is defined as:

$$Q = \frac{N_y - N_x}{N_y + N_x} \qquad (3)$$

where N_x represents the double event counts along the direction parallel to the polarisation field vector and N_y is the counts in the orthogonal direction. An orthogonal asymmetry is quite evident, also by eyes, in the counts detected by pixels surrounding the target. The beam polarisation plane is oriented along the horizontal direction of the image and, as expected, the counts are higher in the vertical direction. Selecting from the data the double events, it is possible to built scattering distribution maps using the distance vector between the two energy deposits and taking the beam target pixel as the reference position.

The accumulation of events with the same second vector coordinates in an array that has the same size as the detector produces the scattering distribution maps (Figure 15). The

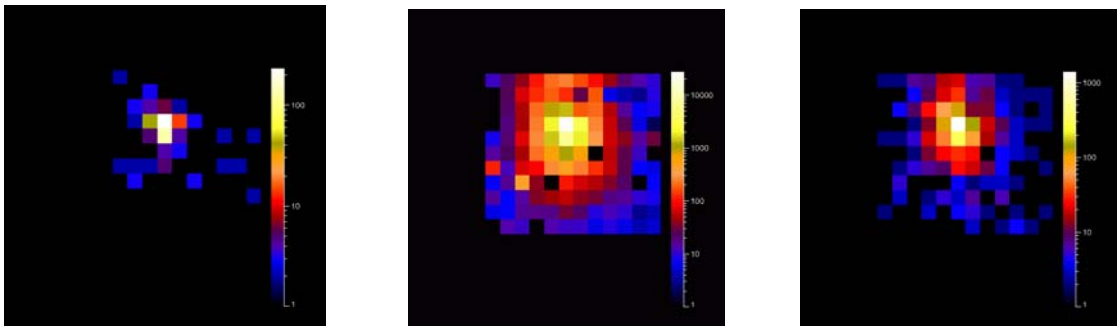

Figure 15. *The distribution of the scattering distance vector of double events hits obtained with 90, 270 and 345 keV (from left to right) diffracted beam impinging on pixel 201. The colour levels are proportional to the logarithmic of contents of each map cell.*

distribution exhibits the expected ellipsoidal shape with the longer axis orthogonal to the photon polarisation vector.

This type of scattering distribution map was produced for each diffracted beam energy and for each Cu crystal position in the simulated Laue lens rings. All distributions were normalized for detection non uniformity using correction factors evaluated by Eq. (1).

From each of these maps the modulation factor Q was evaluated by integrating counts in the two orthogonal directions aligned to the detector sides. The values obtained for the two higher beam energies (270 and 345 keV) are presented in Figure 16. Poor double-event statistics at 90 keV prevent us from deriving accurate results; consequently this data set is not shown. The Q values obtained by this experiment confirm the results from a previous ESRF experiment with the same detector without the use of a Laue diffraction element and are in agreement with expected modulation factor evaluated by MC simulations for the energies used and for equivalent detector geometry (i.e. pixel size and thickness).

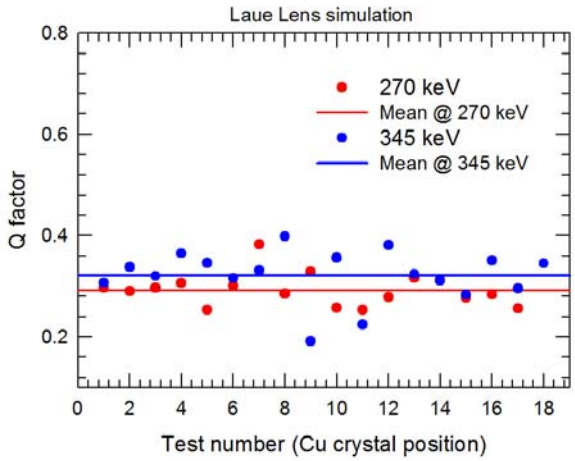

Figure 16. *The modulation factor Q obtained for each Cu crystal position in the Laue lens simulation tests for the higher beam energies. The data errors are of the order of the symbol size.*

4.4 Evaluation of systematic effect of Laue diffraction on polarisation

In order to verify the presence of systematic effects induced by the Laue focusing process some simple statistical tests can be applied to the Q factor series obtained for each energy.

First we have used a simple chi square test (χ^2) to infer the compatibility of the evaluated Q data series with a constant value given by the average value. This test allows us to exclude, at 98% confidence level for 270 keV and 95% for the 345 keV line, any direct correlation and/or trend of the modulation factor Q with respect to the different Cu crystal positions.

Of course this type of test is not very sensitive to periodic structures inside the observed data series, especially if their amplitude is comparable with the statistical errors on the data. A quite simple method that can be used to verify this type of modulation of our Q data series is provided by the Fisher exact test of periodicity [16]. This test uses the Fisher *g*-statistic to infer the statistical significance of the largest periodic component in a data series. This method relies on the computation of the periodogram of the data series, i.e. the power spectral distribution *I(ω)* derived from the discrete Fourier Transform of the data set itself. The I(ω) function for the measured Q data sets is reported in Figure 17.

The second step is the definition of the *g*-statistics of our Q series, by:

$$g = \frac{\max(I(\omega))}{\sum_{k=1}^{(N-1)/2} I(\omega_k)} \qquad (4)$$

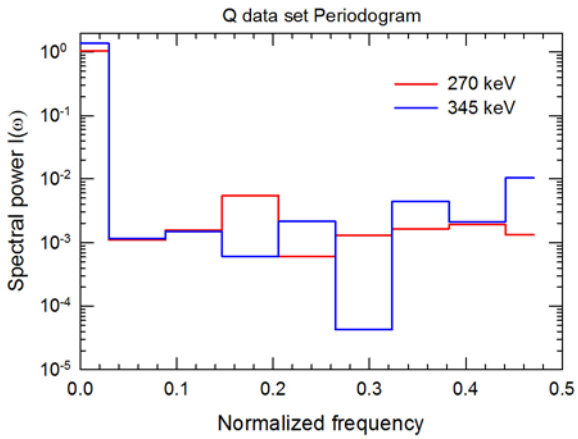

Figure 17 *The discrete spectral power function (periodogram) of the two Q data series obtained at 270 and 345 keV during the Laue lens ring simulation. The normalised frequency in abscissa is simply given by k/N, where k go from 0 to (N-1)/2 and N is the series data number*

where max($I(\omega)$) represent the largest value in the periodogram corresponding to a given discrete frequency, and the denominator is simply the sum of all the spectral powers (excluding the zero frequency corresponding to the Fourier transform constant term). For the two Q series g is equal to 0.3623 and to 0.4632, respectively for data at 270 keV and at 345 keV. Using the definition of exact distribution of the Fisher g-statistic under the null hypothesis that there are no significant periodic components [17], these g values allow us to conclude that, at 95% confidence level, the series are randomly distributed around the mean value. Therefore also this result confirms that the modulation Q factor value is not correlated with the Laue Cu crystal position and rotation: i.e. no significant systematic effects are added by the different Laue diffraction condition.

Acknowledgement

We thank the ESRF for the opportunity given to our group with the approval of the LaPOLCA proposal and for all the support (both financial and technical) **offered for the beam test** campaign. In particular we would like thank Dr. Veijo Honkimäki, responsible of the ID15 beam, and all the ESRF staff for the kind and efficient assistance and the support during the test campaign.

This work was carried out in cooperation between the Departamento de Física, Universidade de Coimbra, Portugal (Unit 217/94), the IASF (Istituto di Astrofisica Spaziale e Fisica Cosmica) Bologna and Palermo, INAF, Italy, the ESRF (Grenoble, France), the Dept. of Physics of Universty of Ferrara (Italy).

The authors want to remind their colleague and friend, Dr Giulio Ventura who died suddenly in December 2007, thanking him for his great contribution to this project.

References

1. E. Caroli, et al., *Nucl. Instr. and Meth. Section A*, **448**, pp 525-530 (2000);
2. R.M. Curado da Silva, *Experimental Astronomy* **15,** pp 45–65, (2003);
3. ESA Gamma ray Lens Report: http://sci.esa.int/science-e/www/object/index.cfm?fobjectid=36959;
4. The GRI–Gamma Ray Imager: http://gri.cesr.fr/documents.html;
5. Frontera, F, et al., SPIE Proceedings on *Space Telescopes and Instrumentation 2008: Ultraviolet to Gamma Ray*, **7011**, pp 70111R, (2008), doi:10.1117/12.790484;
6. E. Caroli, et al., Experimental Astronomy, **20**, pp 341-351, (2006);
7. E. Caroli, et al., Experimental Astronomy, **20**, pp 353-364, (2006);
8. R. M. Curado da Silva, et al., SPIE Proceedings on *X-ray and Gamma-ray instrumentation for Astronomy XII*, **4497**, pp 70-78 (2002);
9. E. Caroli, et al., *Nucl. Instr. and Meth. Section A*, **513**, pp 350-356 (2003);
10. R. M. Curado da Silva, et al., *IEEE Trans. Nucl. Sci.*, **50**, nº 4, pp. 1198-1203 (2003);
11. Curado da Silva, R.M, et al., *IEEE Nuclear Science Symposium Conference Record 2007*, **4**, pp 2545 - 2550 (2007);
12. R.M. Curado da Silva, et al., *Journal of Applied Phyics.*, **104**, p. 084903 (2008);
13. E. Caroli, et al., "Experiment on LAue Cu Lens imaging and POLarimetry with CAdmium telluride Array (LaPOLCA) at ESRF", Internal Report IASF/BO n. 524/2008;
14. E. Caroli, et al., *IEEE Nuclear Science Symposium Conference Record 2008,* pp. 90-95, (2009) doi: 10.1109/NSSMIC.2008.4775131;
15. E. Caroli, et al., *IEEE Trans. Nucl. Sci.*, pp. 1848-1854, (2009), doi: 10.1109/TNS.2009.2021475;
16. S. Wichert, K. Fokianos, K. Strimmer, *Bio informatics,* **20,** p. 5, (2004);
17. R.A. Fisher, *Proceedings of the Royal Society of London*,. A **125**, p. 54 (1929).